UNIVERSITY OF LEEDS

Article:
Fernández, J, Marín, P, Díez, FV et al. (1 more author) (2015) Coal mine ventilation air methane combustion in a catalytic reverse flow reactor: Influence of emission humidity. Fuel Processing Technology, 133. pp. 202-209. ISSN 0378-3820

https://doi.org/10.1016/j.fuproc.2015.02.005

Coal mine ventilation air methane combustion in a catalytic reverse flow reactor: influence of emissions humidity

Javier Fernández, Pablo Marín, Fernando V. Díez, Salvador Ordóñez*

Department of Chemical and Environmental Engineering, Faculty of Chemistry, University of Oviedo, Julián Clavería 8, Oviedo 33006, SPAIN

* Phone: 34-985 103 437, FAX: 34-985 103 434, e-mail: sordonez@uniovi.es

Abstract

The role of the humidity content on the performance of catalytic reverse flow reactors (RFR) for the abatement of methane emissions from coal mines is studied in this manuscript. It has been demonstrated that this technique is very useful for the abatement, and even upgrading, of these emissions. However, the effect of humidity on the reactor performance has not been addresses yet, in spite of being well known that water is an inhibitor in catalytic combustion.

Experimental studies in a lab-scale isothermal fixed bed reactor demonstrated that water decreases the activity of a palladium on alumina catalyst for the combustion of methane, but this inhibition is entirely reversible, results fitting well to a Langmuir-Hinshelwood kinetic model. Then, the influence of water was studied in a bench-scale RFR operating at near adiabatic conditions at different switching times (100-600 s) and methane feed concentrations (2700-7200 ppm). Finally, a mathematical model for the reverse flow reactor, including the kinetic model with water inhibition, has been validated using the experimental results. This model is of key importance for designing this type of reactors for the treatment of mine ventilation emissions.

Keywords: precious metal catalyst; methane deep oxidation; monolithic catalyst; water inhibition; unsteady state reactors; model-based design.

1. Introduction

In the last decades, environmental problems related to global warming have gained importance. Coal mining is an activity with great influence on greenhouse emission, because of the huge amount of methane emitted to the atmosphere during coal extraction through the ventilation system (concentration 1000 to 10 000 ppm). Ventilation air methane represents the main contribution (approximately 78%) to the carbon footprint of coal mining [1].

In the atmosphere, methane is accumulated and slowly oxidized with average lifetime of around 12 years. Nevertheless, the effect of methane as greenhouse gas is 21 times higher than the one of carbon dioxide. For this reason, the combustion of methane to carbon dioxide before release has a great interest to reduce the net warming potential [2, 4].

One suitable option for the treatment of ventilation air methane in coal mining is regenerative oxidation, and in particular regenerative catalytic oxidation (RCO) in a reverse flow reactor [5,6]. Catalytic oxidation is an interesting alternative to thermal oxidation, since the use of a catalyst significantly decreases the ignition temperature and, as a consequence, the size and thermal requirements of the combustion device. Moreover, the formation of NO_x is negligible [7, 8].

Reverse flow reactors (RFR) consist of a catalytic fixed bed reactor in which the feed flow direction is periodically reversed. RFRs present great potential advantages for the combustion of hydrocarbon emissions. By selecting the appropriate switching time (t_{sw}, defined as the time elapsed between two consecutive flow reversals), most of the combustion heat is stored inside the reactor in consecutive cycles, so that autothermal operation is possible even for very slightly exothermic reactions. Hence, RFRs allow the efficient treatment of very lean emissions of volatile organic compounds (VOC) (e.g. originated from the use of organic solvents) or methane (e.g. coal mine vents) in air [9-11].

RFR advantages are a consequence of its forced unsteady state operation. However, this can also be a drawback to maintain ignited operation in the presence of disturbances in the feed flow rate or concentration. For example, if the feed becomes too lean, there is a risk of extinction, because the amount of heat released by the reaction is very low; in these situations, the RFR regeneration

capacity is crucial to maintain autothermal operation. Under rich feed conditions, the heat released and accumulated in the reactor can overheat the catalyst bed, leading to catalyst thermal deactivation. Such issues have limited the industrial use of this type of reactors, and encouraged research in the development of suitable control systems [12-15].

The catalyst performance is affected by the presence of side compounds (different of methane) in the ventilation air. Among these compounds, water stands out because it is commonly present at high concentration in these emissions (near to saturation at ambient temperature). It is well-known that water has a negative effect on the activity of supported precious metal catalysts. The oxidation of methane on palladium-supported catalysts has been studied by different authors, with a general agreement on the existence of a reversible inhibitory effect [16-28]. Models based on Mars-van Krevelen or Langmuir-Hinshelwood kinetics have been found to agree with the observations [17].

The combustion of methane in reverse flow reactors has been studied experimentally, and also by means of simulations. Previous studies have been centred in the influence of operating conditions [19, 20], optimization [21], model validation [20, 22], control of ignition state [13, 23], or heat recovery [14, 24]. Although water is present in high concentration in coal mine ventilation air (20000-50000 ppm) and the performance and stability of reverse flow reactors can be highly affected by the decrease of the catalyst activity caused by water, to the best of our knowledge, this aspect has not been studied. The main objective of this work is to fill this gap and assess the influence of water in the oxidation of methane in catalytic reverse flow reactors.

For accomplishing this purpose, the effect of water on the reaction kinetic is firstly studied, and an appropriate kinetic model is proposed. Then, the influence of water on the performance of reverse flow reactors is analysed in a bench-scale device. Finally, a detailed mathematical model of the reverse flow reactor is proposed and validated with the experimental data. This model is suitable to be used in the design and optimization of commercial-scale devices for the treatment of methane emissions in the presence of water.

2. Methodology

2.1. Catalyst characterization

The catalyst used in this work, representative of catalysts commonly used for methane combustion, is a commercial palladium-based monolith supplied by BASF (reference FP-CPO-5M). The monolithic catalyst is formed by an inert support (cordierite) with a cell density of 390 cpsi (cell size $1.02 \cdot 10^{-3}$ m, open porosity 65% vol.) and a washcoating (average thickness $8.1 \cdot 10^{-5}$ m, fraction 20% vol.) impregnated with the active phase (0.39% wt. palladium). Catalyst geometry was measured directly using the images from a stereomicroscope (Stemi 2000-C, ZEISS).

Solid density (2300 kg/m^3) was measured experimentally, and the solid heat capacity (900 J/kg K) and thermal conductivity (0.8 W/m K) were taken from the literature for cordierite-based monoliths.

Textural characteristics (specific internal surface area and pore volume) were measured by nitrogen adsorption at 77 K in a Micromeritics ASAP 2020 surface area analyser. Obtained data have been used for estimating internal porosity (12% vol.) and porous structure properties (mean pore diameter 12 nm), needed for the mathematical modelling of the reactor.

2.2. Isothermal lab-scale reactor

Catalyst stability and reaction kinetics for methane oxidation have been studied in an isothermal fixed-bed reactor (0.6 m length and $9 \cdot 10^{-3}$ m internal diameter). The monolith was ground and sieved to 100-250 μm, and then mixed with ground glass (355-710 μm) to avoid deviations from plug-flow behaviour (tube diameter/particle diameter > 10).

The required feed methane/air mixture was prepared by mixing an air-methane mixture of 25 000 ppm methane, from a cylinder, and purified air from a compressor (Ingersoll-Rand), using two mass flow regulators. Inlet and outlet streams were analysed in an Agilent gas chromatograph (GC).

Water was introduced in the air stream with the help of a bubbler. The concentration of water was regulated using a temperature control system formed by a heating blanket and a temperature controller. The water content is analysed using a hydrometer (VATSAIA HMI 32).

2.3. Adiabatic bench-scale reverse flow reactor

The bench-scale reverse-flow reactor used in the present work consists of a 0.8 m long 0.05 m internal diameter 316 stainless steel tube. The tube contains three monolithic beds: one catalytic (0.15 m long) situated in the middle, and two inert (0.125 m long each) situated at both ends. The beds are surrounded by a glass wool layer, in order to avoid gas bypass near the reactor wall. The temperature of the bed is measured in 5 points along the reactor axis using a multipoint thermocouple array. The flow reversal is accomplished by using two pairs of solenoid valves (Parker-Lucifer 121K46E), acting on the reactor inlet and outlet streams.

Reactor feed, consisting of methane-air mixtures with different methane concentrations, is set using two mass flow meters (Bronkhorst F201C). The analysis of methane concentration at the inlet and outlet streams is performed on-line (each 5 s) using an infrared spectrometer (ABB- PIR3502). The reactor tube is surrounded by an oven, equipped with a dynamic temperature-control system able of compensating the heat transfer through the reactor tube, and hence allowing a reactor operation close to adiabatic [20,25,26].

The following protocol has been followed for each test. First, the reactor was fed with hot air, in order to pre-heat the beds above the ignition temperature of the air-methane mixture (T_{pre} = 400ºC). Then, the methane/air mixture was fed to the reactor (0.15 m/s n.t.p.) at room temperature (20ºC), and the flow reversal was started. The reactor was then operated until pseudo-steady state or extinction.

2.4. Reverse flow reactor model

Based on previous experience on modelling reverse flow reactors [20, 27-29], in this work, a 1D heterogeneous dynamic model has been selected (see equations in Table 1). The meaning of the symbols is indicated in the list of symbols. The physical and transport properties appearing in the equations of Table 1 must be specified or calculated by means of appropriate correlations, as indicated in a previous work [22]. Danckwerts boundary conditions (see Table 2) have been used to

solve the model in MATLAB using the method of lines (ode15s) [20, 22]. The switch of the feed direction is modelled by shifting the boundary conditions at both sides of the reactor.

3. Results and discussion

3.1. Catalyst stability

Catalyst stability at reaction conditions has been determined in the absence and presence of water. Tests have been carried out in the isothermal fixed-bed reactor at 475ºC and WHSV 1.22 m^3 (n.t.p.) kg_{cat}^{-1} min^{-1} with methane feed concentration 1000 ppm. Results are depicted in Figure 1. In the absence of water, methane conversion decreases during the first 1.5 h and then remains constant. Water is introduced in the reactor at t = 7 h with a concentration of 16000 ppm, causing a sudden drop in conversion from 28% to 21%. Then, conversion remains nearly constant upon time. Finally, when the water feeding is discontinued at t = 13 h, methane original conversion is recovered immediately. This indicates that water causes inhibition of the methane oxidation reaction rather than deactivation of the catalyst, as reported by other authors [17, 30-33].

3.2. Kinetic modelling

In the literature, several kinetic models have been proposed for the oxidation of methane in the presence of water, the most commonly used being power-law, Mars-van Krevelen and Langmuir Hinshelwood models [16, 35]. Langmuir-Hinshelwood models are based on mechanisms where different species (methane, oxygen and water) are adsorbed on the catalyst surface, and the reaction involves adsorbed oxygen and methane. The inhibition caused by water can be explained by competitive adsorption of methane and water. The following kinetic equation can be derived based on this mechanism (the terms corresponding to oxygen, in great excess, in the constants) [34]:

$$-r_{CH_4} = \frac{k_w p_{CH_4}}{1 + K_{H_2O} p_{H_2O}} = k'_w p_{CH_4} \qquad \text{(Eq.1)}$$

Where p_{CH_4} and p_{H_2O} are methane and water gas partial pressure, k_w is the kinetic constant and K_{H_2O} is the adsorption equilibrium constant of water. k_w and K_{H_2O} are assumed to have an exponential dependence with temperature according to Arrhenius and Van't Hoff equations, respectively. Water concentration in the reactor is nearly constant, so the kinetic equation is of first order with respect to methane with apparent kinetic constant k'_w.

The rate of methane oxidation has been measured in the isothermal fixed-bed reactor, operating at WHSV 0.98 m^3 (n.t.p.) kg_{cat}^{-1} min^{-1}. The following expression is obtained by solving the plug-flow reactor model with the previous kinetic model (Eq.1).

$$k'_w = \left(\frac{F_0}{p_0 W}\right) ln\left(\frac{1}{1 - X_{CH_4}}\right) \qquad \text{(Eq.2)}$$

where F_0 is the total molar flow rate, p_0 is the total gas pressure and X_{CH_4} is methane conversion.

Figure 2a shows the light-off curves obtained at different methane feed concentrations (1000-5000 ppm) in the absence of water. The different curves overlap, indicating that conversion is independent of methane concentration, like in Eq.2, and hence that reaction rate is first order on methane partial pressure. The kinetic constants calculated by Eq. 2 are used to calculate the Arrhenius parameters. An activation energy of 80 kJ mol^{-1} was obtained, similar to the values reported in the literature for precious metal-catalysed methane combustion [30, 35].

The absence of diffusional limitations has been checked by calculating the parameters proposed in the literature for the most unfavourable conditions (highest temperature considered in the fitting, 450ºC): Carberry number (external mass transfer) $Ca = r_{obs}/K_G a_S C_G$ = $9 \cdot 10^{-4}$ < 0.05, Wheeler-Weisz criteria (internal mass transfer) $\eta\phi^2 = r_{obs} d_p^2 / D_e C_S$ = $9 \cdot 10^{-2}$ < 0.1, external heat transfer $\left|K_G(-\Delta H) C_G E_a Ca / hRT_G^2\right|$ = $1 \cdot 10^{-3}$ < 0.05 and internal heat transfer $\left|D_e(-\Delta H) C_S E_a \eta\phi^2 / k_e R T_S^2\right|$ = $5 \cdot 10^{-7}$ < 0.05.

Light-off curves obtained for different water feed concentrations (20000 to 50000 ppm) at constant WHSV 1.22 m^3 (n.t.p.) kg_{cat}^{-1} min^{-1} and methane feed concentration 1000 ppm are depicted in Figure 2b. It is clearly observed that water reduces the activity of the catalyst, resulting in a decrease of

methane conversion at all temperatures. Moreover, the inhibition is stronger at high water concentrations.

The parameters of this Eq.1 were fitted to the experimental data by the least-squares method using the EXCEL Solver; the following parameters being obtained: $k_w = 2.44\, e^{-80000/RT}$ mol kg_{cat}^{-1} s^{-1} Pa^{-1} and $K_{H_2O} = 8.07 \cdot 10^{-9}\, e^{67600/RT}$ Pa^{-1} (R = 8.314 J mol^{-1} K^{-1}). These results agree with other published results [17, 36].

Methane conversions predicted by the model with the fitted parameters are depicted in Figure 2b (lines). The model accurately predicts the increase of conversion with temperature for the different water concentrations.

3.3. RFR performance in presence of water

The experiments in the bench-scale reverse flow reactor have been planned according to an experimental design, where the main operating variables are varied within the following ranges: water concentration (20000 - 50000 ppm), methane concentration (2700-7200 ppm) and switching time (100-600 s). The most representative results are compared in Figure 3 and 4 by means of the temperature profiles at the middle of a cycle. These plots are very useful for studying the behaviour of the reactor, being a measurement of the heat released (in the catalytic bed) and stored (in the inert beds) in the reactor. The boundaries of the inert and catalytic beds are indicated by dashed lines.

Figure 3 compares the performance of the reactor at high and low switching times. Switching time determines the amount of heat stored in the reactor between cycles, and used for pre-heating the feed in the next cycle, and for this reason is critical in achieving stable reactor operation (when switching time is too long the reactor cools down gradually and finally extinction occurs). Results show that, as expected, average temperature in the reactor centre are substantially higher for low switching time (100 s) than for high switching time (600 s). As a result, at switching time 600 s stable

reactor operation is only achieved for methane feed concentration above 5400 ppm, while at 100 s the reactor is stable for methane concentrations as low as 3600 ppm.

When the reactor is operated in the presence of water, the temperature plateau decreases; for comparison purposes, the other operating variables are held constant. This can be explained by the inhibition of the catalytic activity towards methane oxidation produced by water, which decreases methane conversion, and hence, the heat released and stored in the reactor. As expected, this effect is more marked at high water gas concentrations, because the catalyst inhibition is stronger.

The influence of methane and water gas feed concentrations are analysed in Figure 4 at constant switching time (300 s). As expected, bed temperature is higher for the experiments at higher methane concentration, and bed temperature decreases with increasing water content. The difference between the experiments with and without water is more marked at high methane concentration. In the test carried out at the highest water concentration (50000 ppm), the inhibition is so strong that the reactor extinguished. These results demonstrate that water affects the thermal stability of the reverse flow reactor and its long-term stable operation, reducing the interval of operating conditions (methane concentration and switching time) for which the reactor operation is stable.

3.4. RFR model validation in the presence of water

The mathematical model presented in the methodology section has been validated by simulating all the experiments and comparing experiments and simulations in terms of temperature and methane conversion.

Typical results are depicted in Figure 5 and 6. The evolution of temperature upon time at three reactor positions (z = 0.050, 0.116 and 0.200 m, measured from a bed end; as the total bed length is 0.400 m, z = 0.200 m corresponds to the reactor centre) is depicted in Figure 5 for two experiments. It must be considered that bed temperature profiles are symmetric due to the periodic behaviour of the reactor. At the beginning of the experiments (t = 0), the reactor bed is pre-heated uniformly to

400ºC. Then, the methane feed is introduced at room temperature and the flow reversal is started. This produces a temperature wave that moves forward and backward along the reactor bed. In the temperature versus time plots, this movement is observed as saw teeth, which are characteristic of the behaviour of reverse flow reactors. The temperature evolution trend in the different reactor positions indicates how the reactor is performing.

The experiment shown in Figure 5 a, c and e is unstable, because temperature decreases upon time in all bed positions (except a slight increase at the beginning at z = 0.200 m) and the reactor proceeds to extinction. In this particular case, methane feed concentration is not enough to achieve long-term stable operation of the reactor with water inhibition. The correspondence between experiments and simulations is good (except at z = 0.200 m, where the model predicts a temperature slightly lower), and the model succeeds in predicting the inhibition and associated temperature decrease caused by water.

The experiment analysed in Figure 5 b, d, f is stable. The evolution of temperature with time shows that the system reaches a stable pseudo-steady state in which the same temperature evolution is repeated after successive cycles. There is good agreement between simulations and experiments, though there are small discrepancies for z = 0.200 m, as in the previous experiment. These discrepancies are explained by a poorer temperature control in the middle of the reactor, because the temperature is higher, which results in deviations from the adiabatic behaviour of the bench-scale reactor. The temperature evolution at the other positions of the reactor is predicted accurately.

Bed temperature profiles are also very useful to determine the validity of the model. In Figure 6, profiles at different stages of a cycle (at beginning, the middle and the end) are compared for experiments and simulations. In general, the model is able of predicting the reactor behaviour. As indicated before, the major discrepancies are found in the bed centre.

In conclusion, the 1D heterogeneous mathematical model with catalyst inhibition proposed in this work can be considered as validated with the experiments carried out in a bench-scale reverse flow reactor operating at near-adiabatic conditions. The simple Langmuir-Hinshelwood kinetic model,

obtained from conventional light-off curves, is useful for modelling methane combustion in the presence of water in RFR. This RFR model can now be used in the design and optimization of RFR commercial-scale units for methane combustion from sources where catalyst inhibition by water is expected, such as coal mine vents and landfill lean emissions, among others.

3.5. Considerations for the design of a RFR in the presence of water

This section is devoted to the study of the RFR stability at different operating conditions and its consequences in the design of commercial scale units. In Figure 7, all the experiments carried out in this work are depicted as a function of the operating conditions (switching time and methane feed concentration) for the case of (a) water-free conditions and (b) 40 000 ppm water (corresponding to a relative humidity of 75%). The experiments that resulted in stable operation of the reactor appear at the upper part of the graph with a solid marker; the unstable ones at the bottom with an open marker. A line, obtained by simulations using the mathematical model, determines the limit between the stable and unstable zones. Reactor stability is determined by the combination of the heat released by the reaction (given by methane concentration) and switching time; reactor stability increasing for higher methane concentration and lower switching time. Switching times lower than 50 s are not considered, as they cause important by-pass of un-reacted methane (*wash-out*) as explained in the literature, and mechanical problems (flow reversal valves premature ageing) [10-12]. It can be observed that the presence of water reduces notably the range of operation conditions at which stable operation can be achieved. Thus, for the same switching time an increase of approximately 1500 ppm in the feed concentration is required. The heat released by the additional 1500 ppm increases the catalyst temperature, so that it compensates the decrease in activity caused by water. The same effect can also be achieved by reducing the switching time, which increases the heat trapped in the reactor, and hence the temperature of the catalyst. It should also be considered that the temperature of the catalyst cannot be increased indefinitely to compensate the lower

activity of the catalyst. The catalyst has maximum recommended operating temperature to prevent overheating.

Figure 7 demonstrates that the decrease in catalyst activity caused by water highly affects the performance of the reverse flow reactor, reducing the range of operating conditions in which its stable operation is possible. However, autothermal reactor operation is still possible, by increasing methane feed concentration or, within certain limits, lowering switching time.

4. Conclusions

Coal mine ventilation air contains appreciable amounts of methane, but also water that undoubtedly affects the catalytic combustion of methane and, consequently, the operation of catalytic reverse flow reactors. The aim of this study is to get new insights on the influence of this water on the operation of catalytic reverse flow reactors.

It was found that water produces a reversible inhibition on precious metal-based catalysts, which was successfully modelled using a Langmuir-Hinshelwood kinetic model. The study was extended to a bench-scale reverse flow reactor equipped with a precious-metal based monolithic catalyst, operated at different feed water concentrations. The results of the experiments show that the decrease in the catalyst activity produced by water reduces methane conversion, and hence the heat released in the reactor. This decreases the temperature of the catalytic bed and the stability of the reverse flow reactor.

A mathematical model for the reverse flow monolithic reactor, capable of modelling the inhibition caused by water, was proposed and validated with the experimental data. This model is very useful for the study of the influence of reactor design and operating conditions on the reactor performance and the design of commercial scale reverse flow reactors. It was demonstrated that the design of efficient reactors in the presence of water in the feed requires special attention. As an illustration, the operating conditions (methane and water concentration and switching time) resulting on stable RFR operation or reaction extinction were determined for a particular reactor design, showing that

the effect of water can be overcome by increasing methane concentration or decreasing switching time.

Acknowledgements

This work was supported by the Research Fund for Coal and Steel of the European Union (contract UE-10-RFCR-CT-2010-00004). The samples of the monolithic catalyst were kindly supplied by BASF.

Nomenclature

a	geometric external surface to volume ratio (m^2/m^3_{bed})
C	molar concentration (mol/m^3)
C_P	heat capacity (J/kg k)
D	diffusion coefficient (m^2/s)
E_a	Activation energy (kJ/mol)
F_0	total molar flow rate (mol/s)
h	gas to solid heat transfer coefficient (W/m^2 K)
k	thermal conductivity (W/m K)
K_G	gas to solid mass transfer coefficient (m/s)
K_{H_2O}	adsorption equilibrium constant for water (Pa^{-1})
k_w	kinetic constant (mol/kg_{cat} s Pa)
p	pressure (Pa)
r	reaction rate (mol/kg_{cat} s)
R	ideal gas constant (8.314 J/mol K)
t	time (s)
T	temperature (K)
t_{sw}	switching time (s)
u	gas superficial velocity (m/s)
W	catalyst weight (kg)

X	conversion (-)
y	molar fraction (-)
z	spatial coordinate (m)

Greek symbols

ΔH	heat of reaction (J/mol)
ϵ_b	bed porosity (-)
ϕ	Thiele modulus (-)
η	internal effectiveness factor of the catalyst (-)
ρ	density (kg/m^3)

Subscripts

0	inlet
ax	axial
e	effective
G	gas
S	solid

Caption to figures

Figure 1 Catalyst stability at constant reaction conditions: 475ºC, 1000 ppm methane, WHSV 1.22 m^3 (n.t.p.) kg_{cat}^{-1} min^{-1}. (◆) methane conversion. (▬) water concentration (ppm).

Figure 2 Light-off curves of the ground monolith at different conditions.

(a) Methane feed concentration: (■) 1000 ppm, (✕) 2000 ppm, (◆) 3000 ppm, (△) 5000 ppm. WHSV = 0.98 m^3 (n.t.p.) kg_{cat}^{-1} min^{-1}. No water.

(b) Water feed concentration: (◆) 3000, (▲) 8000, (■) 15000, (●) 23000 and (✕) 33000 ppm. WHSV = 1.22 m^3 (n.t.p.) kg_{cat}^{-1} min^{-1}. 1000 ppm methane.

Figure 3 Temperature profiles in the reverse flow reactor at mid cycle. Influence of the water feed concentration: (■) 0, (◆) 30000 and (▲) 40000 ppm.

(a) t_{sw} = 600 s, y_{G0} = 5400 ppm.

(b) t_{sw} = 100 s, y_{G0} = 3600 ppm.

Figure 4 Temperature profiles in the reverse flow reactor at mid cycle: influence of the water feed molar fraction: (■) 0, (◆) 30000 and (▲) 40000 ppm.

(a) t_{sw} = 300 s, y_{G0} = 3600 ppm.

(b) t_{sw} = 300 s, y_{G0} = 4500 ppm.

Figure 5 Model validation: evolution of reactor temperature at 0.050, 0.116 and 0.200 m. (▬) Experiment, (▬) simulation.

(a). (c) and (e): y_{G0} = 3600 ppm, t_{sw} = 200 s, y_{H20} = 33000 ppm.

(b). (d) and (f): y_{G0} = 5400 ppm, t_{sw} = 300 s, y_{H20} = 37000 ppm.

Figure 6 Model validation: evolution of temperature profiles during a half-cycle (gas flow from left to right), beginning (◆), middle (■) and end of half-cycle (▲). Symbols: experiments; lines: simulations.

(a). y_{G0} = 3600 ppm, t_{sw} = 200 s, y_{H20} = 33000 ppm.

(b). y_{G0} = 5400 ppm, t_{sw} = 300 s, y_{H20} = 37000 ppm.

Figure 7 Influence of water in the reverse flow reactor performance and stability.

(a). Free of water: stable (◆) and unstable (◇) experiment.

(b). Water concentration = 37000 ppm: stable (▲) and unstable (△) experiment.

Stability limit: free of water (▬ ▬) and water concentration = 37000 ppm (⋯).

Figure 1

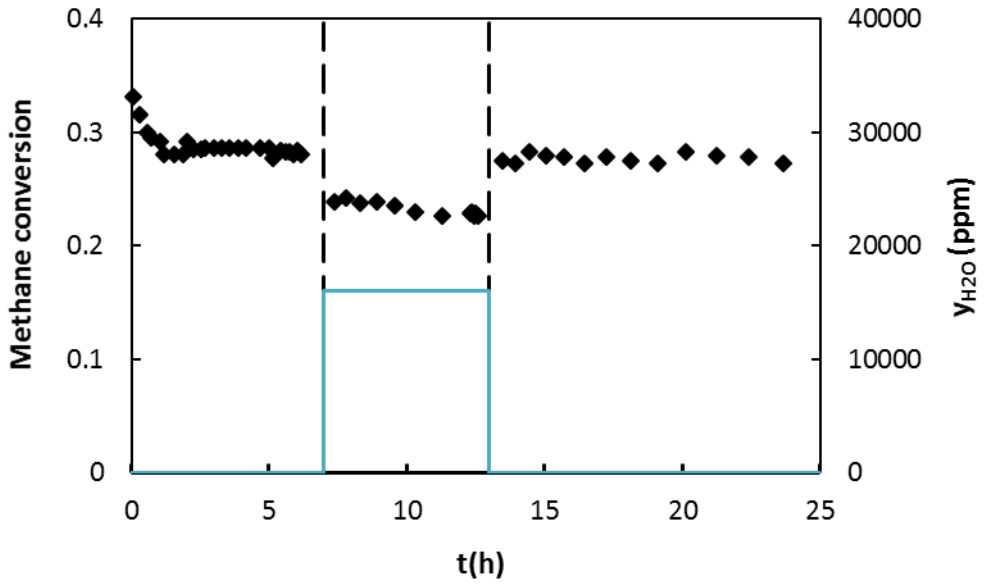
Methane conversion
0.4
0.3
0.2
0.1
0
0
5
10
15
20
25
t(h)
40000
30000
20000
10000
0
y_{H2O} (ppm)

384

385 **Figure 2**

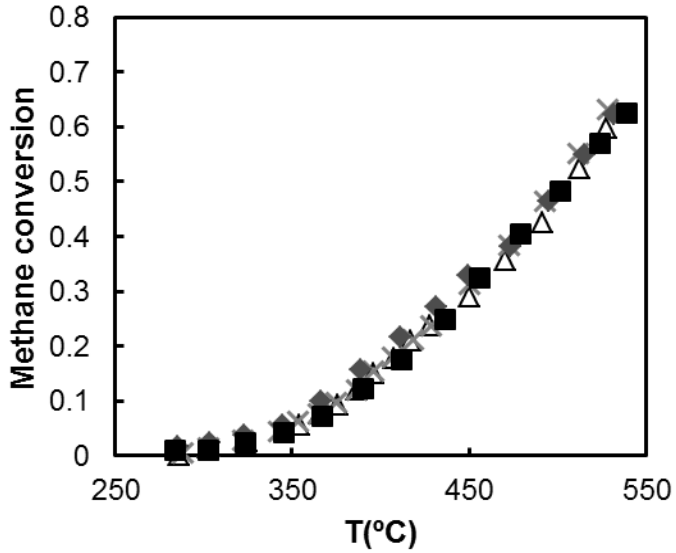

386 **(a)**

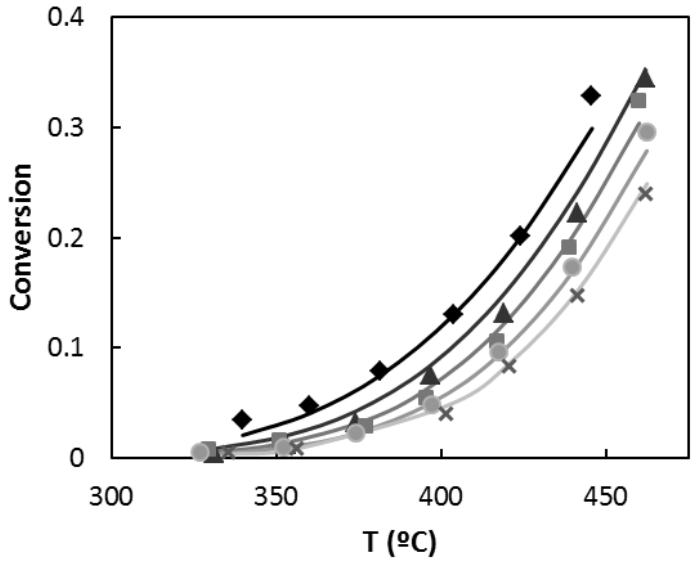

387 **(b)**

388

389

390 **Figure 3**

391

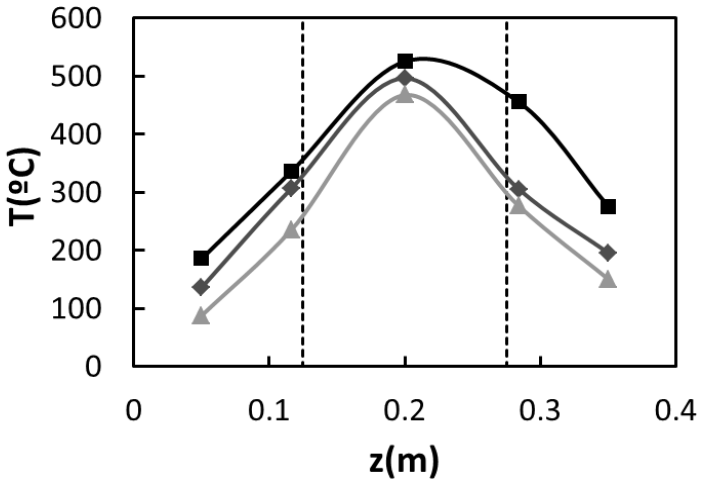

392 **(a)**

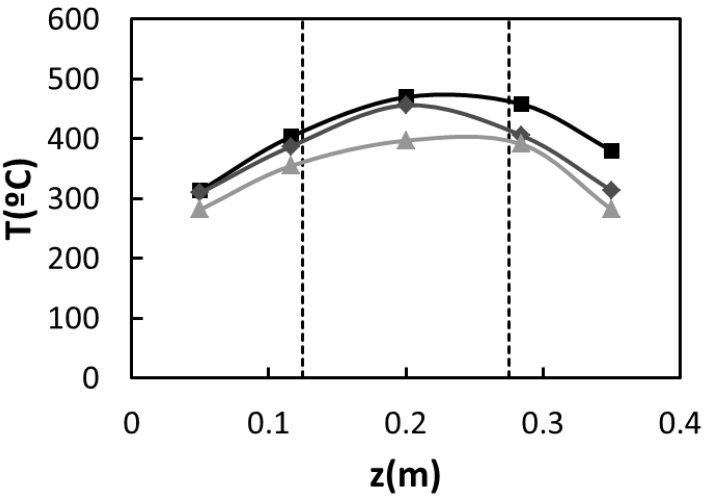

393 **(b)**

394

395

396

Figure 4

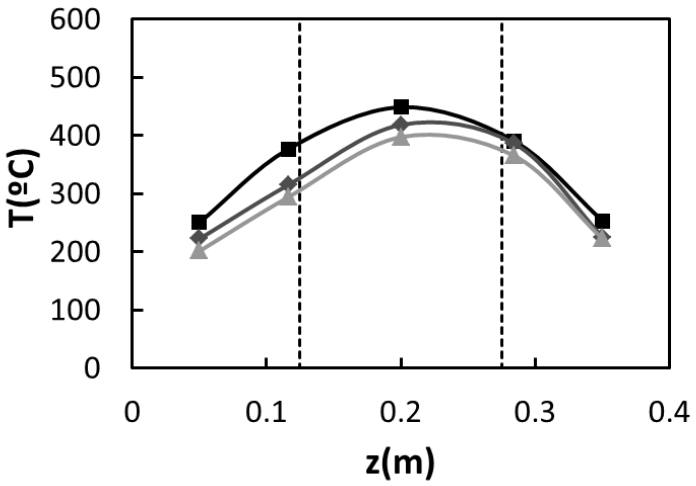
600
500
400
300
200
100
0
T(ºC)
0
0.1
0.2
0.3
0.4
z(m)

(a)

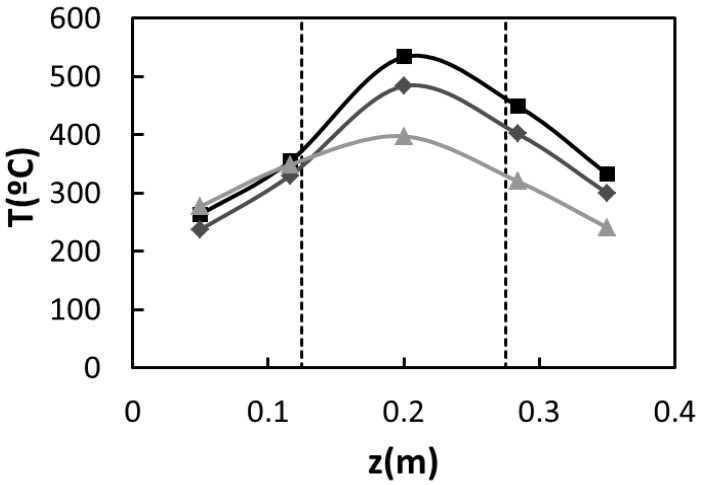
600
500
400
300
200
100
0
T(ºC)
0
0.1
0.2
0.3
0.4
z(m)

(b)

406

407 **Figure 5**

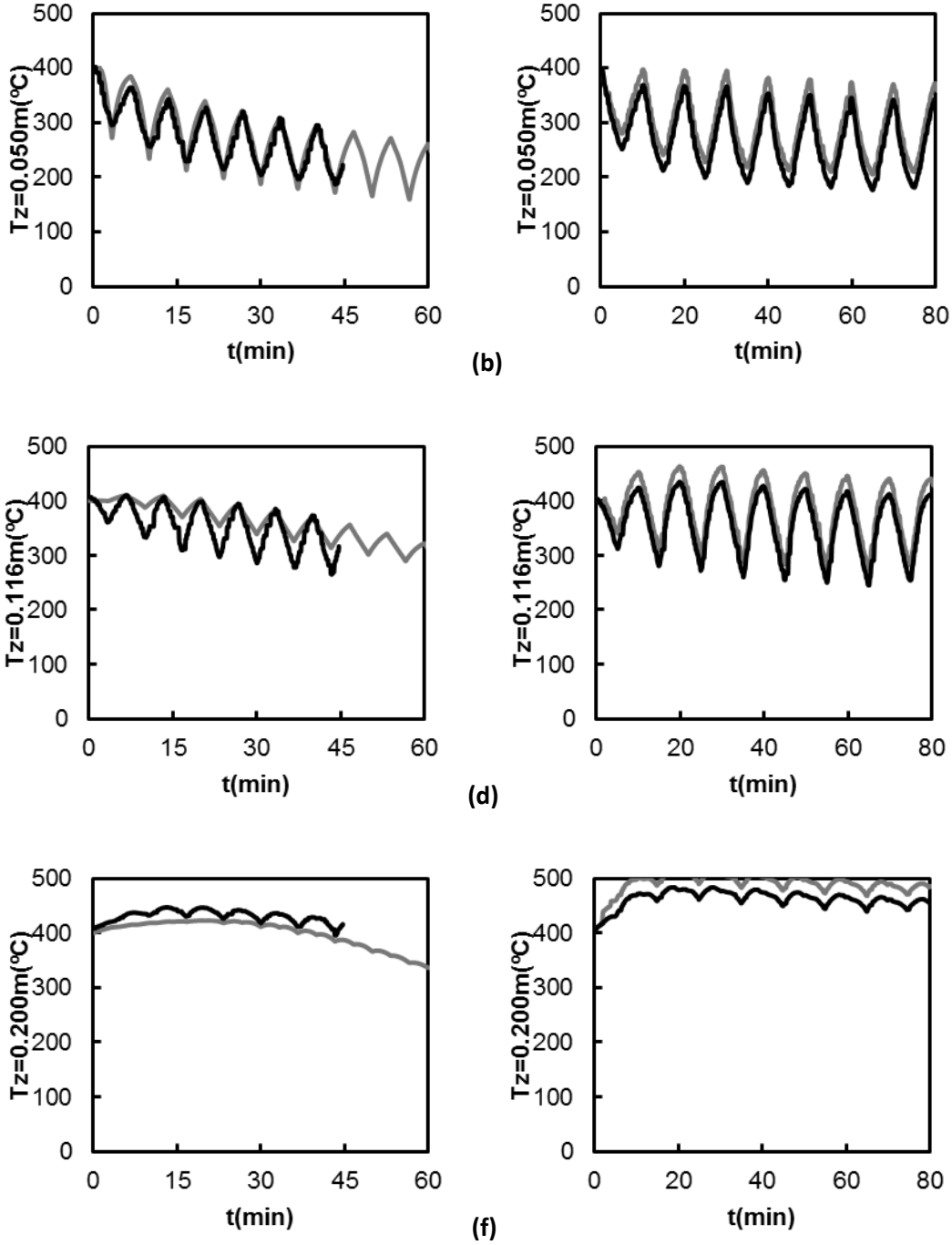

408

409

410

411

412

413

414 **Figure 6**

415

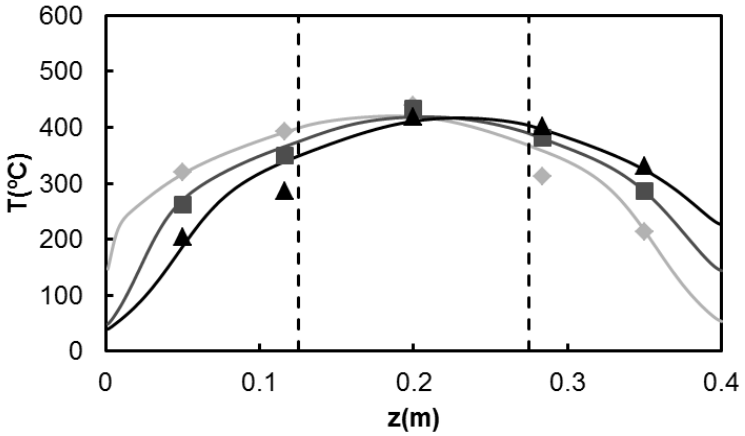

416 **(a)**

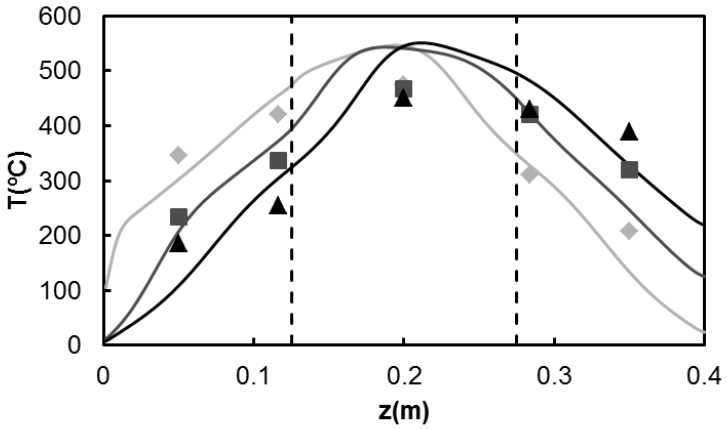

417 **(b)**

418

419

420

Figure 7

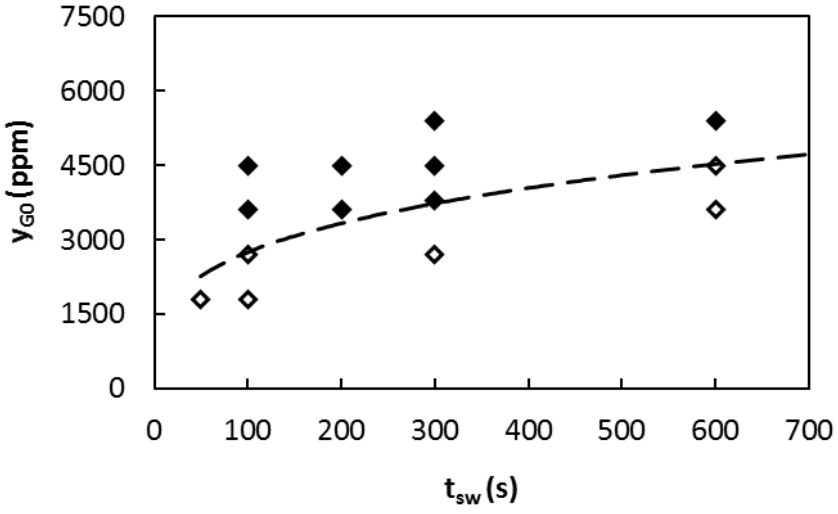
7500
6000
4500
3000
1500
0
0
100
200
300
400
500
600
700
y_{G0} (ppm)
t_{sw} (s)

(a)

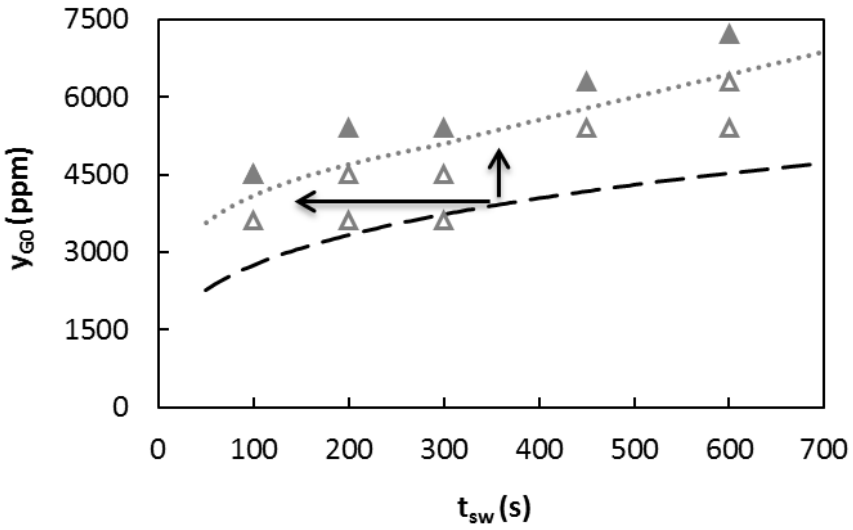
7500
6000
4500
3000
1500
0
0
100
200
300
400
500
600
700
y_{G0} (ppm)
t_{sw} (s)

(b)

List of tables

Table **1**

Mass balance to the gas phase
$$\frac{\partial y_G}{\partial t} = -\frac{u_0}{\epsilon_b}\frac{\rho_{G0}}{\rho_G}\frac{\partial y_G}{\partial z} + D_{ax}\frac{\partial^2 y_G}{\partial z^2} - \frac{aK_G}{\epsilon_b}(y_G - y_S)$$
Mass balance to the solid phase
$$\frac{\partial y_S}{\partial t} = \frac{aK_G}{(1-\epsilon_b)}(y_G - y_S) + \frac{\rho_S \eta r_{CH_4}}{c_G}$$
Energy balance to the gas phase
$$\frac{\partial T_G}{\partial t} = -\frac{u_0}{\epsilon_b}\frac{\rho_{G0}}{\rho_G}\frac{\partial T_G}{\partial z} + \frac{k_{Gax}}{\rho_G C_{PG}}\frac{\partial^2 T_G}{\partial z^2} + \frac{ah}{\rho_G C_{PG}\epsilon_b}(T_S - T_G)$$
Energy balance to the solid phase
$$\frac{\partial T_S}{\partial t} = \frac{k_S}{\rho_S C_{PS}}\frac{\partial^2 T_S}{\partial z^2} + \frac{ah}{\rho_S C_{PS}(1-\epsilon_b)}(T_G - T_S) + \frac{\rho_S \eta r_{CH_4}\Delta H}{\rho_S C_{PS}}$$

446 Table **2**

447

Initial conditions	
$y_G\|_{t=0} = y_S\|_{t=0} = 0$	$T_G\|_{t=0} = T_S\|_{t=0} = T_{ph}$
Boundary conditions	
$(y_{Gj})_{0^-} = (y_{Gj})_{0^+} - \frac{\epsilon_b D_{ax}}{u_0}\left(\frac{\partial y_{Gj}}{\partial z}\right)_{0^+}$	$(T_G)_{0^-} = (T_G)_{0^+} - \frac{\epsilon_b \kappa_{G,ax}}{u_0 \rho_{G0} C_{PG}}\left(\frac{\partial T_G}{\partial z}\right)_{0^+}$
$\left(\frac{\partial y_{Sj}}{\partial z}\right)_{z=0^+} = 0$	$\left(\frac{\partial T_S}{\partial z}\right)_{z=0^+} = 0$
$\left(\frac{\partial y_{Gj}}{\partial z}\right)_{z=L_R} = \left(\frac{\partial y_{Sj}}{\partial z}\right)_{z=L_R} = 0$	$\left(\frac{\partial T_G}{\partial z}\right)_{z=L_R} = \left(\frac{\partial T_S}{\partial z}\right)_{z=L_R} = 0$

448

449

450

References

[1] Díaz E, Fernández J, Ordóñez S, Canto N, González A. Carbon and ecological footprints as tools for evaluating the environmental impact of coal mine ventilation air. Ecological Indicators. 2012;18:126-30.

[2] Su S, Beath A, Guo H, Mallett C. An assessment of mine methane mitigation and utilisation technologies. Progress in Energy and Combustion Science. 2005;31:123-70.

[3] Karacan CÖ, Ruiz FA, Cotè M, Phipps S. Coal mine methane: A review of capture and utilization practices with benefits to mining safety and to greenhouse gas reduction. International Journal of Coal Geology. 2011;86:121-56.

[4] Badr O, Probert SD, O'Callaghan PW. Atmospheric methane: Its contribution to global warming. Applied Energy. 1991;40:273-313.

[5] Su S, Agnew J. Catalytic combustion of coal mine ventilation air methane. Fuel. 2006;85:1201-10.

[6] Warmuzinski K. Harnessing methane emissions from coal mining. Process Safety and Environmental Protection. 2008;86:315-20.

[7] Karakurt I, Aydin G, Aydiner K. Mine ventilation air methane as a sustainable energy source. Renewable and Sustainable Energy Reviews. 2011;15:1042-9.

[8] Gosiewski K, Pawlaczyk A. Catalytic or thermal reversed flow combustion of coal mine ventilation air methane: What is better choice and when? Chemical Engineering Journal. 2014;238:78-85.

[9] Marín P, Ordóñez S, Díez FV. Systematic study of the performance of a reverse flow reactor for the treatment of lean hydrocarbon emissions. Journal of Chemical Technology & Biotechnology. 2009;84:1292-302.

[10] Barresi AA, Baldi G, Fissore D. Forced unsteady-state reactors as efficient devices for integrated processes: Case histories and new perspectives. Industrial & Engineering Chemistry Research. 2007;46:8693-700.

[11] Matros YS, Bunimovich GA. Reverse-Flow Operation in Fixed Bed Catalytic Reactors. Catalysis Reviews. 1996;38:1 - 68.

[12] Marín P, Díez FV, Ordóñez S. A new method for controlling the ignition state of a regenerative combustor using a heat storage device. Applied Energy. 2014;116:322-32.

[13] Marín P, Ho W, Ordóñez S, Díez FV. Demonstration of a control system for combustion of lean hydrocarbon emissions in a reverse flow reactor. Chemical Engineering Science. 2010;65:54-9.

[14] Li Z, Qin Z, Zhang Y, Wu Z, Wang H, Li S, et al. A control strategy of flow reversal with hot gas withdrawal for heat recovery and its application in mitigation and utilization of ventilation air methane in a reverse flow reactor. Chemical Engineering Journal. 2013;228:243-55.

[15] Zhang Y, Doroodchi E, Moghtaderi B. Chemical looping combustion of ultra low concentration of methane with Fe2O3/Al2O3 and CuO/SiO2. Applied Energy. 2014;113:1916-23.

[16] Ciuparu D, Pfefferle L. Support and water effects on palladium based methane combustion catalysts. Applied Catalysis A: General. 2001;209:415-28.

[17] Hurtado P, Ordóñez S, Sastre H, Díez FV. Combustion of methane over palladium catalysts in presence of inorganic compounds: inhibition and deactivation phenomena. Applied Catalysis B: Environmental. 2004;47:85-93

[18] Zhang Y, Doroodchi E, Moghtaderi B. Chemical looping combustion of ultra low concentration of methane with Fe2O3/Al2O3 and CuO/SiO2. Applied Energy. 2014; 113:1916-23.

[19] Salomons S, Hayes RE, Poirier M, Sapoundjiev H. Flow reversal reactor for the catalytic combustion of lean methane mixtures. Catalysis Today. 2003;83:59-69.

[20] Marín P, Ordóñez S, Díez FV. Monoliths as suitable catalysts for reverse-flow combustors: modelign and experimental validation. AIChE Journal. 2010;56:3162-73.

[21] Litto R, Hayes RE, Sapoundjiev H, Fuxman A, Forbes F, Liu B, et al. Optimization of a flow reversal reactor for the catalytic combustion of lean methane mixtures. Catalysis Today. 2006;117:536-42.

[22] Thompson CR, Marín P, Díez FV, Ordóñez S. Evaluation of the use of ceramic foams as catalyst supports for reverse-flow combustors. Chemical Engineering Journal. 2013;221:44-54.

[23] Balaji S, Fuxman A, Lakshminarayanan S, Forbes JF, Hayes RE. Repetitive model predictive control of a reverse flow reactor. Chemical Engineering Science. 2007;62:2154-67.

[24] Marín P, Ordóñez S, Díez FV. Procedures for heat recovery in the catalytic combustion of lean methane-air mixtures in a reverse flow reactor. Chemical Engineering Journal. 2009;147:356-65.

[25] Marín P, Ordóñez S, Díez FV. Rational design of heating elements using CFD: Application to a bench-scale adiabatic reactor. Computers & Chemical Engineering. 2011;35:2326-33.

[26] Fissore D, Barresi AA, Baldi G, Hevia MAG, Ordóñez S, Díez FV, AIChE Journal. 2005; 51: 1654-64.

[27] van de Rotten BA, Verduyn Lunel SM, Bliek A. Efficient simulation of periodically forced reactors with radial gradients. Chemical Engineering Science. 2006;61:6981-94.

[28] Liu B, Hayes RE, Yi Y, Mmbaga J, Checkel MD, Zheng M. Three dimensional modelling of methane ignition in a reverse flow catalytic converter. Computers & Chemical Engineering. 2007;31:292-306.

[29] Marín P, Hevia MAG, Ordóñez S, Díez FV. Combustion of methane lean mixtures in reverse flow reactors: Comparison between packed and structured catalyst beds. Catalysis Today. 2005;105:701-8.

[30] Abbasi R, Wu L, Wanke SE, Hayes RE. Kinetics of methane combustion over Pt and Pt–Pd catalysts. Chemical Engineering Research and Design. 2012;90:1930-42.

[31] Gao D, Wang S, Zhang C, Yuan Z, Wang S. Methane Combustion over Pd/Al2O3 Catalyst: Effects of Chlorine Ions and Water on Catalytic Activity. Chinese Journal of Catalysis. 2008;29:1221-5.

[32] Persson K, Pfefferle LD, Schwartz W, Ersson A, Järås SG. Stability of palladium-based catalysts during catalytic combustion of methane: The influence of water. Applied Catalysis B: Environmental. 2007;74:242-50.

[33] Zhang B, Wang X, M'Ramadj O, Li D, Zhang H, Lu G. Effect of water on the performance of Pd-ZSM-5 catalysts for the combustion of methane. Journal of Natural Gas Chemistry. 2008;17:87-92.

[34] Liu B, Hayes RE, Checkel MD, Zheng M, Mirosh E. Reversing flow catalytic converter for a natural gas/diesel dual fuel engine. Chemical Engineering Science. 2001;56:2641-58.

526 [35] Hurtado P, Ordóñez S, Sastre H, Díez FV. Development of a kinetic model for the oxidation of
527 methane over Pd/Al2O3 at dry and wet conditions. Applied Catalysis B: Environmental. 2004;51:229-
528 38.

529 [36] Gosiewski K, Matros YS, Warmuzinski K, Jaschik M, Tanczyk M. Homogeneous vs. catalytic
530 combustion of lean methane—air mixtures in reverse-flow reactors. Chemical Engineering Science.
531 2008;63:5010-9.

532

533